Reprinted from SPIE Vol. 540—Southwest Conference on Optics

Tests of the Algorithm for the Calculation of Scattering by a Multilayered Sphere

Ramesh Bhandari

Applied Laser/Optics Group, Physics Department
Box 3D, New Mexico State University, Las Cruces, New Mexico 88003

Abstract

For numerical tests of the calculational procedure for scattering by a multilayered sphere, absorption of visible light by graphitic carbon (soot) mixed with nonabsorbing or weakly absorbing material like water is calculated. Three cases of mixing within the framework of the multilayered model are considered: (1) carbon exists as a tiny core within a water droplet, (2) carbon exists as a thin shell on the outside of the water droplet, and (3) carbon exists as a thin shell within the water droplet (double-layered case). Numerical calculation of absorption cross sections is performed, treating the carbon content in each case as a perturbation in the Mie scattering of light by a homogeneous sphere of water. The results obtained agree perfectly with those obtained directly by the use of algorithms based on the exact expressions.

I. Introduction

In the preceding paper[1], we proposed a calculational procedure for light scattering by a multilayered sphere with an arbitrary number of layers. In this paper, we describe some numerical tests of the calculational procedure. The tests are based on the concept that when one of the layers is thin, the scattering by a multilayered sphere is reduced to scattering by a multilayered sphere with one less layer (the thin layer), the thin layer acting only as a perturbation. The same argument holds if the inner most core of the sphere is tiny. In either case, a direct computation of scattering using the calculational procedure of Ref. 1 must yield results corresponding to the perturbative approach.

We begin by stating the exact analytic expressions for scattering by a single-layered case in Section II, and subsequently report the results for the case of a tiny core embedded at the center of a sphere in Section III, followed by the results for the case of a thin shell around a spherical particle in Section IV. Section V discusses the case of a thin concentric shell of a different material within an otherwise homogeneous sphere (a double-layered case). For each of these cases, numerical results are given for absorption of visible light by water droplets contaminated with graphitic-carbon (soot) (existing as a tiny core or thin shell as discussed above).

II. Single-Layered Sphere

According to the results of Ref. 1, the partial-wave scattering amplitudes for a plane-wave incident on a single-layered sphere (Fig. 2 of Ref. 1) can be written as[2]

$$a_n = \frac{N_n}{D_n} \tag{1}$$

$$b_n = \frac{M_n}{C_n} \tag{2}$$

where

$$N_n = \begin{vmatrix} \psi_n(x_2) & m_2\psi_n(m_2x_2) & m_2\chi_n(m_2x_2) & 0 \\ \psi_n'(x_2) & \psi_n'(m_2x_2) & \chi_n'(m_2x_2) & 0 \\ 0 & m_2\psi_n(m_2x_1) & m_2\chi_n(m_2x_1) & m_1\psi_n(m_1x_1) \\ 0 & \psi_n'(m_2x_1) & \chi_n'(m_2x_1) & \psi_n'(m_1x_1) \end{vmatrix} \tag{3}$$

$$D_n = \begin{vmatrix} \zeta_n(x_2) & m_2\psi_n(m_2x_2) & m_2\chi_n(m_2x_2) & 0 \\ \zeta_n'(x_2) & \psi_n'(m_2x_2) & \chi_n'(m_2x_2) & 0 \\ 0 & m_2\psi_n(m_2x_1) & m_2\chi_n(m_2x_1) & m_1\psi_n(m_1x_1) \\ 0 & \psi_n'(m_2x_1) & \chi_n'(m_2x_1) & \psi_n'(m_1x_1) \end{vmatrix} \quad (4)$$

$$M_n = \begin{vmatrix} \psi_n(x_2) & \psi_n(m_2x_2) & \chi_n(m_2x_2) & 0 \\ \psi_n'(x_2) & m_2\psi_n'(m_2x_2) & m_2\chi_n'(m_2x_2) & 0 \\ 0 & \psi_n(m_2x_1) & \chi_n(m_2x_1) & \psi_n(m_1x_1) \\ 0 & m_2\psi_n'(m_2x_1) & m_2\chi_n'(m_2x_1) & m_1\psi_n'(m_1x_1) \end{vmatrix} \quad (5)$$

$$C_n = \begin{vmatrix} \zeta_n(x_2) & \psi_n(m_2x_2) & \chi_n(m_2x_2) & 0 \\ \zeta_n'(x_2) & m_2\psi_n'(m_2x_2) & m_2\chi_n'(m_2x_2) & 0 \\ 0 & \psi_n(m_2x_1) & \chi_n(m_2x_1) & \psi_n(m_1x_1) \\ 0 & m_2\psi_n'(m_2x_1) & m_2\chi_n'(m_2x_1) & m_1\psi_n'(m_1x_1) \end{vmatrix} \quad (6)$$

$$x_i = 2\pi\, r_i/\lambda \quad (7)$$

where λ is the wavelength of the incident wave and r_1, r_2 the inner and outer radii of the shell, respectively. m_1 and m_2 denote the refractive indices of the material in the core and within the shell, respectively. The Ricatti-Bessel functions are

$$\begin{aligned} \psi_n(z) &= zj_n(z) \\ \chi_n(z) &= -zn_n(z) \\ \zeta_n(z) &= zh_n^{(2)}(z) \end{aligned} \quad (8)$$

where j_n, n_n, $h_n^{(2)}$ are the spherical Bessel, Neumann, and the Hankel function of the second kind, respectively.

The extinction cross section, the scattering cross section, and the absorption cross section are calculated from a_n and b_n in the following way:

$$\begin{aligned} \sigma_{ext} &= \frac{\lambda^2}{2\pi} \sum_{n=1}^{\infty} (2n+1)\, \mathrm{Re}(a_n + b_n) \\ \sigma_{sca} &= \frac{\lambda^2}{2\pi} \sum_{n=1}^{\infty} (2n+1)\, (|a_n|^2 + |b_n|^2) \\ \sigma_{abs} &= \sigma_{ext} - \sigma_{sca} = \frac{\lambda^2}{2\pi} \sum_{n=1}^{\infty} (2n+1)\, \{\mathrm{Re}(a_n + b_n) - (|a_n|^2 + |b_n|^2)\} \end{aligned} \quad (9)$$

III. Tiny core radius

Assuming $|m_1|\, x_1 << 1$ and $|m_2|\, x_1 << 1$, the Ricatti-Bessel functions with the arguments m_1x_1 and m_2x_1 in Eqs. (3) - (6) can be expanded around zero[3]. Retaining the most leading term in the expansion Eq. (9) reduces to

$$\sigma_{ext} = \sigma_{ext}^{(h)} + 3\lambda^2/2\pi\ \mathrm{Re}(f_1), \tag{10a}$$

$$\sigma_{sca} = \sigma_{sca}^{(h)} + 3\lambda^2/2\pi\ 2\mathrm{Re}((a_1^{(h)})^*\ f_1), \tag{10b}$$

$$\sigma_{abs} = \sigma_{abs}^{(h)} + 3\lambda^2/2\pi\ \mathrm{Re}\{f_1(1-2(a_1^{(h)})^*)\} \tag{10c}$$

where

$$f_1 = -\, m_2\, (\beta_1/\alpha_1)/(D_1^{(h)})^2\ , \tag{11}$$

$$\beta_1/\alpha_1 = i\,\frac{2}{3}\,\frac{(m_2x_1)^3\,(m_1^2 - m_2^2)}{(m_1^2 + 2\,m_2^2)} \tag{12}$$

The superscript h refers to scattering by a homogeneous sphere characterized by parameters m_2, x_2.

$$a_1^{(h)} = N_1^{(h)}/D_1^{(h)} \tag{13}$$

where

$$N_1^{(h)} = \psi_1(x_2)\ \psi_1'(m_2x_2) - m_2\ \psi_1'(x_2)\psi_1(m_2x_2)\ ,$$

$$D_1^{(h)} = \zeta_1(x_2)\ \psi_1'(m_2x_2) - m_2\ \zeta_1'(x_2)\psi_1(m_2x_2). \tag{14}$$

f_1 is the correction term to the scattering amplitude $a_1^{(h)}$, as a result of the tiny core. The correction terms for the remaining amplitudes, $a_n^{(h)}$ and $b_n^{(h)}$, are of higher order in x_1 and neglected. The quantity β_1/α_1 corresponds to Rayleigh scattering amplitude for a plane wave travelling in continuous homogeneous medium with refractive index m_2 and incident on a tiny homogeneous sphere (parameters m_1, x_1) embedded in such a medium. If one further recognizes that $i/D_1^{(h)}$ = the coefficient associated with the field inside a homogeneous sphere (parameters m_2, x_2), the factor $-\,(1/D_1^{(h)})^2$ in the expression for f_1 may be interpreted as a necessary modification to β_1/α_1, since the wave incident on the core (radius r_1) is not the initial plane-wave but the field inside the larger sphere (radius r_2). Moreover, the wave scattered by the core is not being detected within the medium of refractive index m_2, but outside of the larger sphere where the refractive index is 1. This also explains the extra factor of m_2 in Eq. (11) (see the Fresnel coefficient for transmission of light[4]).

If m_2 is real, $\sigma_{abs}^{(h)} = 0$ and Eq. (10c) reduces to

$$\sigma_{abs} = \frac{(3\lambda^2)}{2\pi} m_2\ \mathrm{Im}\ \left\{\frac{-(2/3)\ (m_2x_1)^3\ (m_1^2 - m_2^2)}{m_1^2 + 2m_2^2}\right\}\ \frac{1}{|D_1^{(h)}|^2} \tag{15}$$

which corresponds to absorption in the Rayleigh region modified by factors as discussed earlier.

One of the quantities of interest in the study of the effect of mixing of absorbing material with a non-absorbing material is the absorption cross section per unit volume (or mass) of the absorbing material. Denoting the volume of the absorbing material by V and using Eq. (15), one obtains

$$\sigma_{abs}/V = \frac{-6\pi\ m_2^4}{\lambda}\ \mathrm{Im}\ \left\{\frac{(m_1^2 - m_2^2)}{m_1^2 + 2m_2^2}\right\}/\ |D_1^{(h)}|^2 \tag{16}$$

which is independent of the size of the core, a familiar result in Rayleigh scattering. As an illustration, we consider the absorption of visible light by a tiny graphitic-carbon (soot) core at the center of a water droplet. This is a case of practical interest in the study of scattering of light by fog or clouds. For calculations, we choose $r_2 = 5\mu m$, $\lambda = 0.5\mu m$, m_2 (water) = 1.33-i0·00, and let $m_1 = 2.0 - im_I$. For the special case of soot, we take $m_I = 0{\cdot}66$. Fig. 1 shows the plot of σ_{abs}/V as a function of the volume fraction F of absorbing material for different values of m_I. The top curve corresponds to absorption by graphitic-carbon (soot). Each curve was obtained by using the exact analytic expressions for a single-layered sphere given in Sec. II. The numerical procedure employed is the procedure suggested in Ref. (1). We see in Fig. 1 that the common characteristics of the curves is a flatness in the value of σ_{abs}/V which sets in below $F = 10^{-7}$. This regime corresponds to Rayleigh scattering as can be seen by evaluating m_2x_1. For $F = 10^{-7}$, $m_2x_1 = 0.4$. The limiting value in each curve is precisely the value one obtains from Eq. 16. Considering the tiny amount of absorptive material, this agreement certainly gives confidence in the numerical stability of our computational procedure outlined in Ref. (1). One also remarks here that Eq. (16) predicts the limiting value to be essentially proportional to m_I, which is verified in Fig. 1.

Equation (16) also shows that the dependence of σ_{abs}/V on the outer radius r_2 is expressed through the factor $1/|D_1^{(h)}|^2$, where $D_1^{(h)}$ is given by

$$D_1^{(h)} = \zeta_1(x_2)\psi_1'(m_2x_2) - m_2\zeta_1'(x_2)\psi_1(m_2x_2) \tag{17}$$

In the limit $x_2 >> 1$, this expression reduces to

$$D_1^{(h)} = -e^{-ix_2}\left((\mathrm{Sin}(m_2x_2) - im_2\,\mathrm{Cos}(m_2x_2)\right) \tag{18}$$

Furthermore, when m_2 is real,

$$1/|D_1^{(h)}|^2 = 1/\left[1 + (m_2^2 - 1)\,\mathrm{Cos}^2(m_2x_2)\right] \tag{19}$$

which implies that extrema occur in the value of σ_{abs}/V whenever $m_2x_2 = (2n+1)\,\pi/2$ or $n\pi$ where n is an integer. Fig. 2 shows the plot of σ_{abs}/V as a function of r_2 for $r_1 = 0.0046\ \mu m$, $m_I = 0.66$ with the rest of the parameters being the same as the earlier ones. Calculations again were carried out based on the exact expressions of Sec. II and the calculational procedure of Ref. (1). $m_2x_1 = 0.077$, implying the core is always in the Rayleigh region. Consequently, Eq. (16) remains valid. In Fig. 2, we see the oscillations predicted by Eq. (19). The first prominent peak corresponds roughly to $m_2x_2 = 3\pi/2$, consistent with the fact that x_2 is much greater than 1. Subsequent peaks are given by $m_2x_2 = (2n+1)\,\pi/2$, n = 2,3,4. This oscillating pattern continues beyond $r_2 = 1\mu m$. The distance between any two consecutive peaks is given by $\Delta r_2 = \lambda/(2m_2) = 0.19\mu m$, and the ratio of the maximum to the minimum is $m_2^2 = 1.77$. These results are verified in Fig. 2. The mean value in the region of oscillations is around $23\ m^2/cm^3$ which is to be compared with a maximum value of $13\ m^2/cm^3$ in a polydispersion of carbon particles in air.[5,6] The maximum value corresponds to a carbon particle radius of about $0.08\mu m$.

In Fig. 3, the flatness approached by the curve near the lower end of the curve is due to the onset of Rayleigh scattering for the composite particle and is described by the expression

$$\sigma_{abs}/V = \frac{-54\pi m_2^2}{\lambda(2+m_2^2)^2}\ \mathrm{Im}\left\{\frac{m_1^2 - m_2^2}{m_1^2 + 2m_2^2}\right\} \tag{20}$$

which is obtained from Eq. (16) after making the appropriate approximation for $D_1^{(h)}$. For the parameters considered for the curve in Fig. 2, the value from Eq. (20) is $10.3 m^2/cm^3$ which is in agreement with the limiting value indicated by the curve in Fig. 3. However, if r_2 is decreased further to a value close to r_1 (see Fig. 4), σ_{abs}/V approaches the value corresponding to Rayleigh absorption by carbon particle in air or vacuum (m_2=1). This limit is given by Eq. (20) with $m_2 = 1$. The value is $8.4\ m^2/cm^3$ and agrees with the curve of Fig. 4.

IV. Thin Shell

In this section, we explore the consequences of a thin shell around a spherical particle.

When the shell thickness is small, all the Ricatti-Bessel functions and their derivatives involving the size-parameter x_1 in Eqs. (3-6) can be expanded around the size parameter x_2 in a Taylor's expansion. Writing $x_1 = x_2 - \varepsilon$ and utilizing the differential equation

$$G_n''(z) + (1-n(n+1)/z^2)G_n(z) = 0, \tag{21}$$

where $G_n(z) = \psi_n(z)$, $\chi_n(z)$ in the expansion, one obtains for real m_1

$$\sigma_{abs} = -\varepsilon\lambda^2 A/(2\pi) \tag{22}$$

where

$$A = \sum_n (2n+1)\ \mathrm{Im}\left[(m_2^2 - m_1^2)\left[\{(\psi_n'(m_1x_2))^2 + (n(n+1)/(m_2^2x_2^2))(\psi_n(m_1x_2))^2\}/|D_n^{(h)}|^2 + (\psi_n(m_1x_2))^2/|C_n^{(h)}|^2\right]\right] \tag{23}$$

Note that the factors $1/|D_n^{(h)}|^2$ and $|1/C_n^{(h)}|^2$ are the modulus-squared of the internal field coefficients corresponding to the $a_n^{(h)}$ and $b_n^{(h)}$ scattering amplitudes, respectively. They occur because the shell is embedded in a homogeneous spherical medium of refractive index m_1. When $m_1 = 1$, each one of them reduces to 1. Again, the quantity absorption cross section per unit volume (or mass) of the absorbing material can be evaluated. For σ_{abs} of Eq. (22), σ_{abs}/V is given by

$$\sigma_{abs}/V = -\pi A/(\lambda x_2^2) \ , \tag{24}$$

which is independent of ε, and a constant for a given set of parameters: m_1, m_2, x_2. For the sake of illustration, we consider again the case of a water droplet ($m_1 = 1.33\text{-}i0{\cdot}0$) with graphitic-carbon (soot) ($m_2 = 2.0 - i0{\cdot}66$) this time forming a thin shell on the outside. We take $\lambda = 0.5\mu m$ and $r_2 = 5\mu m$ in the calculations. The calculations are performed using the exact equations (see Sec. II) and the numerical procedure given for the general case of a multilayered sphere in Ref. (1). The results are shown in Fig. 5. The top curve corresponds to the soot material. The other two curves are for different values of the imaginary part of the refractive index of the shell, as further illustration. In each curve flatness, as expected from Eq. (24), is reached below $F = 10^{-6}$. The limiting values in Fig. 5 again agree very well with those predicted by Eq. (24). In addition, they are seen to be proportional to the imaginary part of the refractive index m_2 in agreement with Eq. (23). The peaks are due to a resonance explained below.

We next plot σ_{abs}/V as a function of the outer radius r_2 for a given volume fraction F. We take a low value such as $F = 10^{-7}$ so that Eq. (24) would remain essentially valid during the plot. Eq. (23) shows that as r_2 is varied a pattern analogous to Mie scattering for a homogeneous sphere (characterized by parameters m_2, x_2) will emerge. In Fig. 6 we do see the ripple structure, which is expected considering the range of r_2. The radius r_2 is given increments of 0.01 μm in the plot. When the increment is reduced to 0.0002 μm, we obtain a plot shown in Fig. 7 for a narrow range of r_2 centered about 5μm. More details are visible here than in the previous plot. The peaks are due to resonances in the homogeneous water sphere. The partial wave amplitudes in which they occur are indicated in the figure. The peaks of Fig. 5 are due to the effect of the a_{76} resonance in the immediate vicinity of $r_2 = 5\mu m$.

V. Double-Layered Sphere

The general case of a double-layered sphere is discussed and shown in Ref. 1. However, our purpose here is to consider the spherical case of a thin concentric layer of refractive index m_2, outer radius r_2, embedded in an otherwise homogeneous sphere of refractive index m_1 and radius r_3. Following the approximation procedure for the thin shell in the single-layered case, one obtains exactly the same expression for σ_{abs} (Eq. 22), assuming m_1 is real. However, the functions $D_n^{(h)}$ and $C_n^{(h)}$ in Eq. 23 are now given by

$$D_n^{(h)} = \zeta_n(x_3)\ \psi_n'(m_1x_3) - m_1\zeta_n'(x_3)\ \psi_n(m_1x_3) \ ,$$

$$C_n^{(h)} = m_1\zeta_n(x_3)\ \psi_n'(m_1x_3) - \zeta_n'(x_3)\ \psi_n(m_1x_3). \tag{25}$$

The absorption cross section per unit volume of the absorbing (thin-shell) material is

$$\sigma_{abs}/V = -\pi A/(\lambda\ x_2^2) \ . \tag{26}$$

Clearly, the value of σ_{abs}/V will change as the radius r_2 of the shell is varied within the sphere of radius r_3. Assuming that the shell is a soot shell ($m_2 = 2.0 - i0.66$) within a water droplet ($m_1 = 1.33 - i0.0$) of radius 5μm, results are shown for σ_{abs}/V as a function of r_2 in Fig. 8. The volume fraction is fixed at $F = 10^{-7}$. Calculations are carried out using the exact expressions and the calculational procedure of Ref. 1. Exactly the same curve is obtained when Eq. (26) is used. Before carrying out calculations Eq. (23) in conjunction with Eq. (25) is cast into a form involving logarithmic derivatives and ratios of Ricatti-Bessel functions discussed in Ref. 1. The reproduction of the curve of Fig. 8 by the perturbation approach gives further confidence in the calculational procedure of Ref. 1.

The oscillatory behavior in Fig. 8 is due to the fact that $r_3 \sim 5\mu m$ corresponds to the resonance condition in the partial wave amplitudes a_{76} and b_{66} (see Fig. 7). This leads to high values of the internal field coefficient modulus-squared, $1/|D_{76}^{(h)}|^2$ and $1/|C_{66}^{(h)}|^2$, in Eq. (23). As a result, the oscillatory behavior of $\psi_n(m_1x_2)$ and $\psi_n'(m_1x_2)$ shows up prominently for $n = 76$ and 66. This occurs appropriately at $m_1x_2 \sim n$ (see Fig. 8).

Conclusion

The tests provided here have centered on the ability of the calculational algorithm of Ref. 1 to extract a very small value of the absorption cross section due to the presence of a tiny amount of an absorbing material like graphitic carbon (soot) in a water droplet. The absorptive material exists either as a core or a shell within or on the outside of the water droplet. In each case, comparison with the results based on the perturbative approach shows that the small values of the absorption cross section are accurately calculated. A low volume fraction such as 10^{-7} was used specifically to permit a comparison with the perturbative approach. It should be pointed out, however, that the results given for the shell case are not practically meaningful as a volume fraction as low as 10^{-7} corresponds to a layer with thickness much less than an angstrom.

References

1. R. Bhandari, Proc. of the Southwest Conference on Optics, Albuquerque, NM, 1985.
2. The superscripts of Ref. 1 are now suppressed in the notation: a_n and b_n for the scattering amplitudes, and similarly for other quantities which follow.
3. M. Abramowitz and I. A. Stegun, "Handbook of Mathematical Functions", Dover, New York (1964).
4. M. Kerker, The Scattering of Light and Other Electromagnetic Radiation, Academic, New York (1969); C. F. Bohren and D. R. Huffman, Absorption and Scattering of Light by Small Particles, Wiley, New York (1983).
5. D. M. Roessler, D.S.Y. Wang, and M. Kerker, Appl. Opt. 22, 3648 (1983).
6. P. Chylek and R. Bhandari, Appl. Opt., submitted for publication.

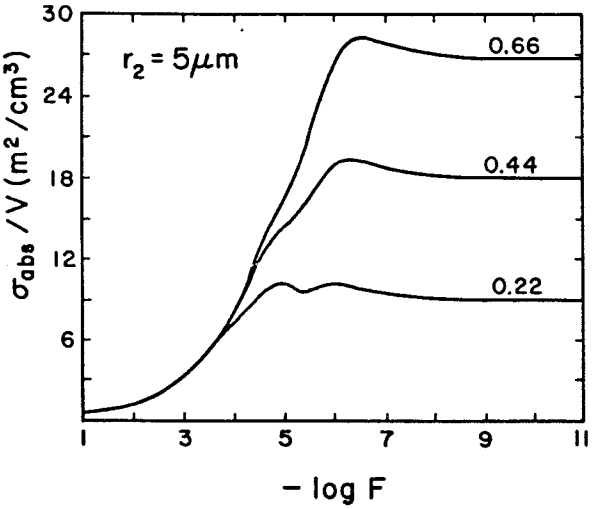

Fig. 1. Absorption cross section/unit volume as a function of volume fraction F of core.

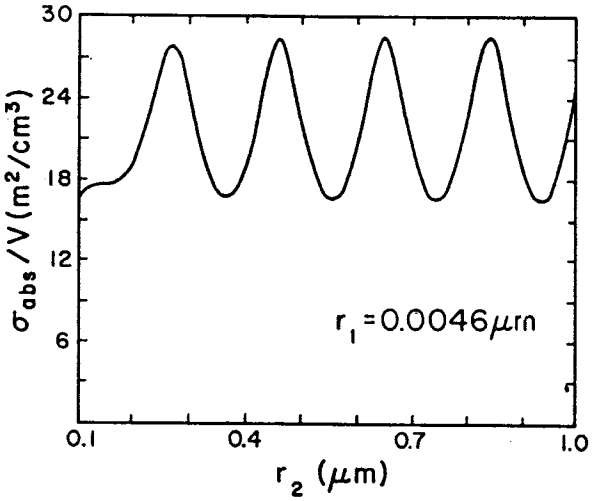

Fig. 2. Absorption cross section/unit volume as a function of the outer radius r_2.

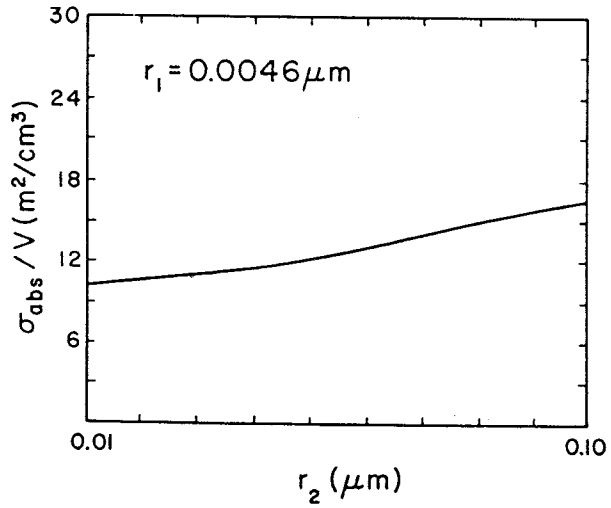

Fig. 3. Same as Fig. 2, but in a low r_2 region.

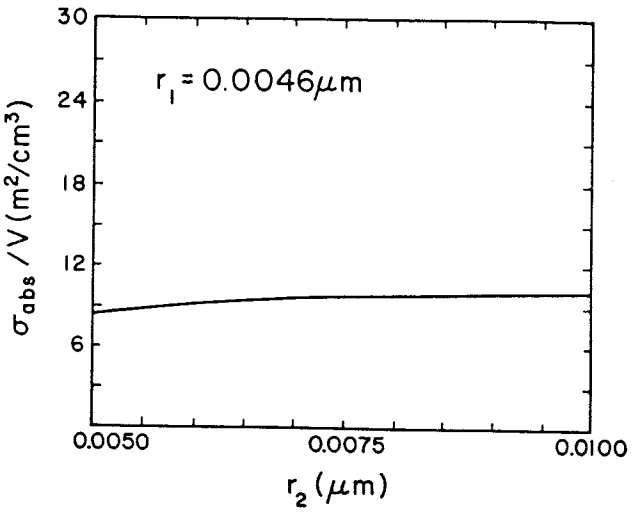

Fig. 4. Same as Fig. 3, but in a still lower r_2 region.

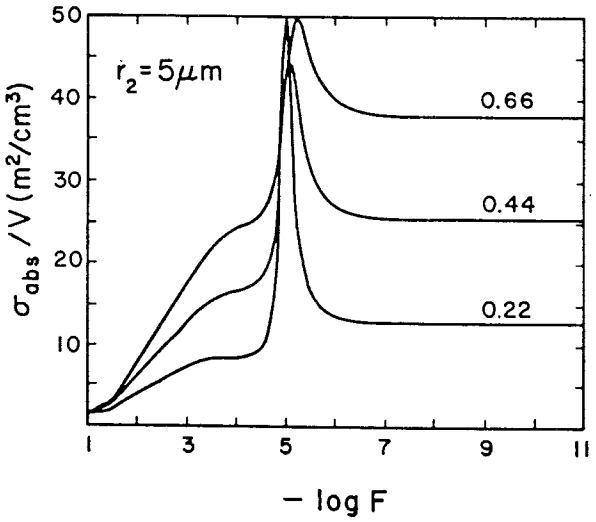

Fig. 5. Absorption cross section/unit volume as as function of volume fraction F of the shell.

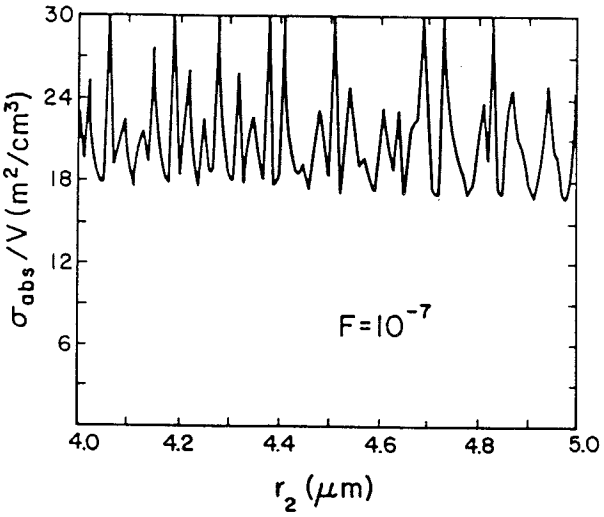

Fig. 6. Absorption cross section/unit volume as a function of the outer radius r_2.

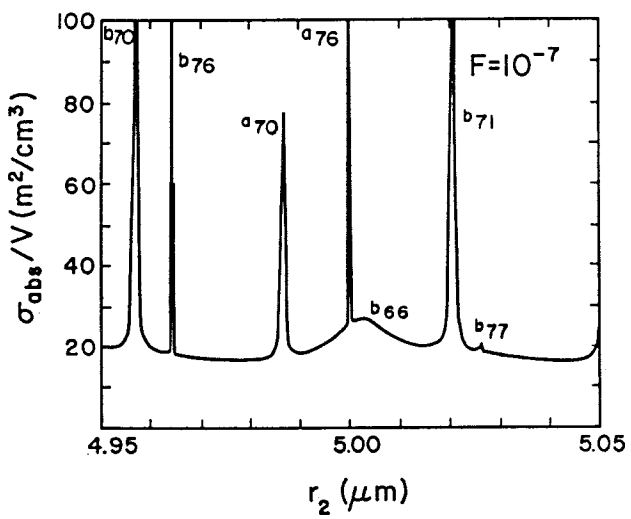

Fig. 7. Same as Fig. 6, but in a narrow range of r_2.

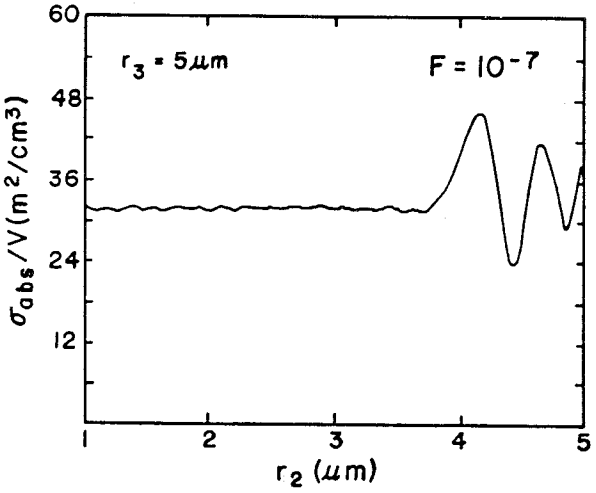

Fig. 8. Absorption cross section/unit volume as a function of the inner shell radius r_2.